Wind and Structures, *Vol. 30, No. 6 (2020) 649-662*
DOI: https://doi.org/10.12989/was.2020.30.6.649

Non-uniform wind environment in mountainous terrain and aerostatic stability of a bridge

Xingyu Chen[1], Junjie Guo[1], Haojun Tang*[1], Yongle Li[1] and Lei Wang[2]

[1]*Department of Bridge Engineering, Southwest Jiaotong University, Chengdu 610031, China*
[2]*Broadvision Engineering Consultants, 650041 Kunming, China*

(*Received November 5, 2019, Revised February 16, 2020, Accepted February 20, 2020*)

Abstract. The existence of a dam has potential effects on the surrounding wind environment especially when it is located in mountainous areas. In this situation, the long-span bridge over the reservoir can easily be exposed to non-uniform incoming flows, affecting its wind-resistance performance. This paper presents a study on the aerostatic stability of such a bridge. Wind tunnel tests were first carried out to investigate the wind environment above a mountainous reservoir. The results show that the angle of attack and the wind speed along the bridge axis show obvious non-uniform characteristics, which is related to the inflow direction. When winds come from the south where the river is winding, the angle of attack varies along the span direction significantly. The finite element model for the bridge was established using ANSYS software, and effects of non-uniform wind loads on the aerostatic stability were computed. Non-uniform angle of attack and wind speed are unfavorable to the aerostatic stability of the bridge, especially the former. When the combined action of non-uniform angle of attack and wind speed is considered, the critical wind speed of aerostatic instability is further reduced. Moreover, the aerostatic stability of the bridge is closely related to the dam height.

Keywords: Aerostatic stability; wind characteristics; non-uniform inflow; dam; mountainous terrains; long-span bridge

1. Introduction

Wind environment is closely related to the aerostatic and the aerodynamic performance of long-span bridges. The existence of mountains has potential effects on the surrounding wind environment, which has attracted great attention. Earlier studies mainly focused on one or two simplified hills or ridges, including theoretical studies (Hunt et al. 1988, Mason and Sykes 1979), field measurement (Mason and King 1985, Mitsuta et al. 1983), wind tunnel tests (Cao and Tamura 2006, Ferreira et al. 1991), and numerical simulations (Cao et al. 2012, Kim et al. 1997), and have greatly improved our understanding of the change in wind environment.

Recently, natural and complex terrains are taken into account. Even in coastal areas, the existence of hills has obvious effects on the wind environment (Bilal et al. 2016, Blocken et al. 2015, Hui et al. 2009). In complex mountainous areas, however, strong winds along rivers are easier to block and deflect by mountains. Wind parameters like the velocity, the angle of attack, and the yaw angle show more complex spatial distributions, that is, the non-uniform characteristics. Li *et al.* (2017) investigated the wind characteristics around the Dadu River Bridge by both wind tunnel tests and numerical simulations, and concluded that the distributions of the wind speed and the angle of attack along the bridge axis are largely affected by the local terrains. Li *et al.* (2017) also investigated the wind characteristics along the girder of the Longjiang Bridge spanning a deep-cutting canyon by wind tunnel tests, and showed that the transverse wind speeds perpendicular to the bridge axis show a negative correlation with the angle of attack. Lystad *et al.* (2018) investigated the wind characteristics along the girder of the Hardanger Bridge by field measurement spanning a fjord surrounded by high and steep mountains, and the mean wind velocity and along-wind turbulence intensity displayed non-uniform characteristics along the girder. Ren *et al.* (2018) established a prediction model based on the correlation of simulation results and illustrated that the model has the ability of predicting the time series of the wind velocity of the spatial wind field under complex terrain. Guignard *et al.* (2019) investigated the variations of the daily means of wind velocity measured by 293 stations in mountainous areas.

In the non-uniform incoming flow, the aerostatic and the aerodynamic performance of long-span bridges may change due to the variation of wind speed and angle of attack along the span. (e.g. Hu *et al.* 2019, Tang *et al.* 2018). Generally, the aerodynamic stability is governing for the design. Since the collapse of the original Tacoma Narrows Bridge, the flutter stability of bridges has attracted great attention. With the increase in bridge span, however, the aerostatic problem also becomes prominent. The critical wind speed of the aerostatic instability is shown to be further reduced when accounting for the varying wind conditions along the bridge span and the material nonlinearities (Boonyapinyo et al. 2006). More importantly, the aerostatic response of long-span bridges is obvious, so the relative angle of attack

*Corresponding author, Ph. D. Lecturer
E-mail: thj@swjtu.edu.cn

ISSN: 1226-6116 (Print), 1598-6225 (Online)

between the bridge and the incoming flow changes, which affects the flutter stability of these bridges. Although the flutter stability may be the governing phenomenon for long-span bridges, it is necessary to understand the aerostatic stability with non-uniform wind environment.

The aerostatic instability of bridges refers to the bending and torsion of the main girder under the given wind speed, which will not only change the structural stiffness and wind loads, but also increase the deformation of the stiffening girder, and eventually lead to the aerostatic instability of the stiffening girder. Cheng *et al.* (2002, 2003) put forward an incremental double iteration method to calculate the critical wind speed of aerostatic instability, which is used widely. Xiao and Cheng (2004) used the non-linear method to analyze the aerostatic stability of Humen Bridge, and explained the aerostatic failure mechanism of suspension bridges by tracing aerostatic instability path. Zhang *et al.* (2013) investigated the mechanism of torsional stiffness degeneration of the cable system and aerostatic torsional divergence of long-span suspension bridges based on a generalized model. Zhang (2007) studied the aerostatic stability of the Runyang Yangtze River Bridge. The results showed that the non-uniform distribution of wind speed along the vertical direction has some influence on the lateral displacement and torsion angle of the bridge, which should be considered in the aerostatic instability analysis. Xu *et al.* (2016) studied the aerostatic stability of the Hutong Bridge, taking into account the variation of wind speed along the altitude, but did not consider the variation of wind speed along the span. Zhang *et al.* (2013b) studied the effects of wind speed spatial non-uniformity on the aerostatic stability of the Maanshan Bridge, and the results showed that the spatial non-uniformity of wind speed has considerable effects on the aerostatic stability of suspension bridges with multiple main spans. However, none of the above studies considers the spatial inhomogeneity of wind speed and angle of attack at the same time. On the other hand, the flutter performance of the structure will also be affected. This is because the position without aerostatic displacement is usually chosen as the equilibrium position of flutter analysis, while the inhomogeneous aerostatic displacement will impose different additional angles of attack along the bridge span, thus changing the flutter performance. Tang *et al.* (2018) investigated the effects of wind velocity distribution, angle of attack, and wind direction on flutter performance of a long-span suspension bridge under non-uniform incoming inflows by the finite element software ANSYS. It is found that the flutter stability of the bridge decreases as the increase in non-uniformity of inflow.

When a long-span bridge crosses the dam and reservoir area, it will be exposed to a complex wind environment. Dams are the water retaining structure that restricts the river and raises the water level. Reservoirs created by dams can regulate the water volume and be beneficial to human activities like irrigation, power generation, aquaculture, and flood control. In Southwest China, many dams have been built along narrow rivers for producing electric power owing to the large drop in altitude. These dams are generally located between two huge mountains and have great heights, and the risen water level leads to wide reservoirs. As a result, long-span suspension bridges are frequently considered when crossing such places. For instance, the Dadu River Bridge with a main span of 1100 m is located at the upstream side of a dam with a distance of about 2.7 km (Li et al. 2017), and the Jinsha River Bridge with a main span of 766 m is located at the upstream side of a proposed dam with a distance of 1.9 km (Wang et al. 2017). Apparently, the existence of a tall dam changes the local wind environment (Jing et al. 2019), and further affects the aerostatic and the aerodynamic performance of the nearby long-span bridge.

Motivated by the remaining problems discussed above, this paper presents a study on aerostatic stability of a long-span suspension bridge with non-uniform wind environment in mountainous area. The content is organized into three more sections: firstly, in Section 2, a long-span suspension bridge located in mountainous terrains was selected as the research object, and the effects of a dam on non-uniform characteristics of inflow are studied by wind tunnel tests. Then Section 3 is devoted to investigation of the aerostatic stability of the bridge with non-uniform inflow by a nonlinear method using the ANSYS Parametric Design Language (APDL) technology, considering the non-uniform angle of attack and non-uniform wind speed. Finally, in Section 4 conclusions are outlined, which can provide some reference for wind-resistant stability of bridges near dams in mountainous terrains.

2. Non-uniform wind characteristics

2.1 Engineering background

The target bridge is a suspension bridge with a main span of 1386 m, and a steel truss stiffening girder is adopted due to the limitation of construction and transportation. The bridge is located in Southwest China and surrounded by huge mountains of which some altitudes exceed 3,011 m, as shown in Fig. 1. The heights of the bridge towers at the west and the east sides are 200.5 m and 230.5 m, respectively. The bridge spans a deep-cutting gorge, and the distance from the bridge deck to the water surface is about 335 m, as shown in Fig. 2. The upstream valley of the dam is straight, basically north-south, while the downstream valley of the dam is winding. Besides the complex natural environment, it is worth noting that there is a dam with a distance of 1,000 m downstream from the bridge site. The construction of the dam makes the upstream water level of the dam site rise significantly, which may provide some shelter for incoming flows from the south and create some local turbulence.

In summary, the bridge is so long that the flexible structure is sensitive to the wind loads, and its wind-resistant performance becomes a key factor in the design. On the other hand, the wind environment around the bridge site is largely determined by the complex terrains and the dam, which is different from the situation of cross-sea bridges. Therefore, it is necessary to investigate the non-uniform wind environment and the effect on the wind-resistant performance of the bridge.

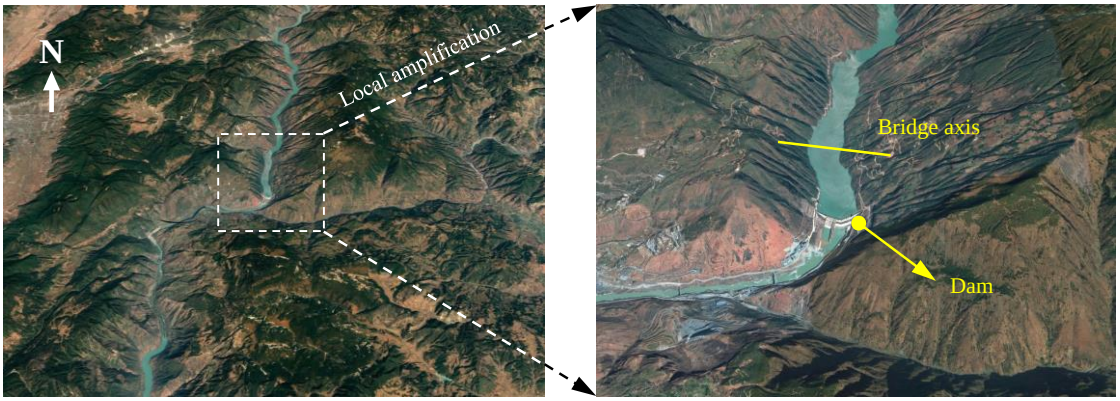

Fig. 1 The bridge site in mountainous canyon areas (topography excerpted from Google Earth)

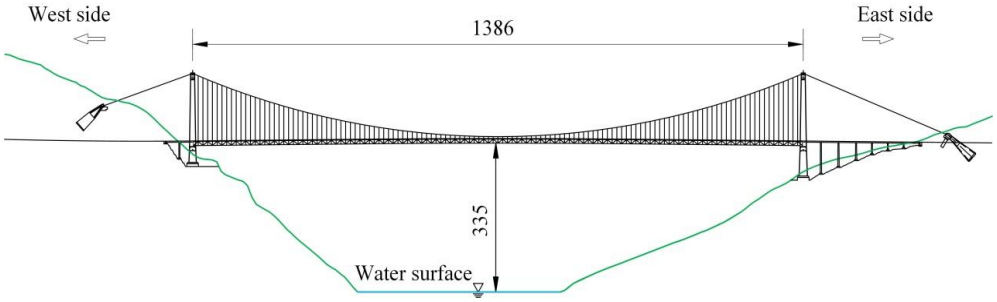

Fig. 2 General arrangement of the suspension bridge

2.2 Terrain model

In order to determine the non-uniform wind characteristics around the bridge site, experimental tests were carried out in XNJD-3 wind tunnel at Southwest Jiaotong University. The dimension of the test section is 4.5 m × 22.5 m × 36.0 m (height × width × length). Considering the size of the wind tunnel and the topographic fluctuation of the real bridge site area, the range covered by the terrain model should be increased as much as possible. Taking the bridge site as the center, the terrain model was made into a circular area with a diameter of 18 km and a scale ratio of 1/2000, as shown in Fig. 3. The model was cut and superimposed by KT boards layer by layer based on the topographic contour, and the height of each board was 5 mm near the bridge site while 10 mm far from it. In order to consider the variation of wind characteristics at the bridge site with the direction of inflow, several pulleys were pre-installed under the model, which can rotate around the center of the model under the action of external forces.

The model edge had a variable height from the tunnel ground determined by the limited size of the terrain model, leading to flow separation around it. It is a common question in the study of wind characteristics in mountainous areas through terrain model test or numerical simulation. In order to transfer the inflow to the model area smoothly, 48 transition sections with varying heights were set at the boundary of the terrain model with reference to the research by Hu *et al.* (2015), as shown in Fig. 3. The adopted curved transition section had a better flow transition performance and made the flow in the tests approach the conditions in full-scale as much as possible. Three cobra probes were employed to measure three-dimensional wind speeds, i.e., the transverse, the bridge-axial, and the vertical wind speeds, which are represented by u, v, and w, respectively. The precision of wind speed is usually ±0.5 m/s, which is very suitable for the measurement of turbulent flow and unknown wind direction. The angle of attack is defined as $\alpha = \tan^{-1}(w/|u|)$, where a positive value means that the incoming flow is upward. By adding spires and roughness blocks on the upstream side of the terrain model, the atmospheric boundary layer in the tests was simulated according to type IV representing very rough terrains in the Chinese code (Ministry of Transport of the People's Republic of China, 2018).

In the wind tunnel tests, different directions of incoming flow were achieved by rotating the terrain model, and six cases were set according to the mountains around the bridge site, as shown in Fig. 4(a). More concretely, the wind directions of cases N1 and S3 were parallel to the river on the upstream side and the downstream side of the bridge, respectively. Case S1 was perpendicular to the southeast ridge of the bridge. Cases N2 and S2 were perpendicular to the bridge axis. Along the bridge axis, nine measurement points at intervals of an eighth of the main span were set. These points were numbered from 1 to 9 where No. 1 presents the position of the tower on the west side; No. 5 is the center of the span; and No. 9 presents the position of the tower on the east side, as shown in Fig. 4(b).

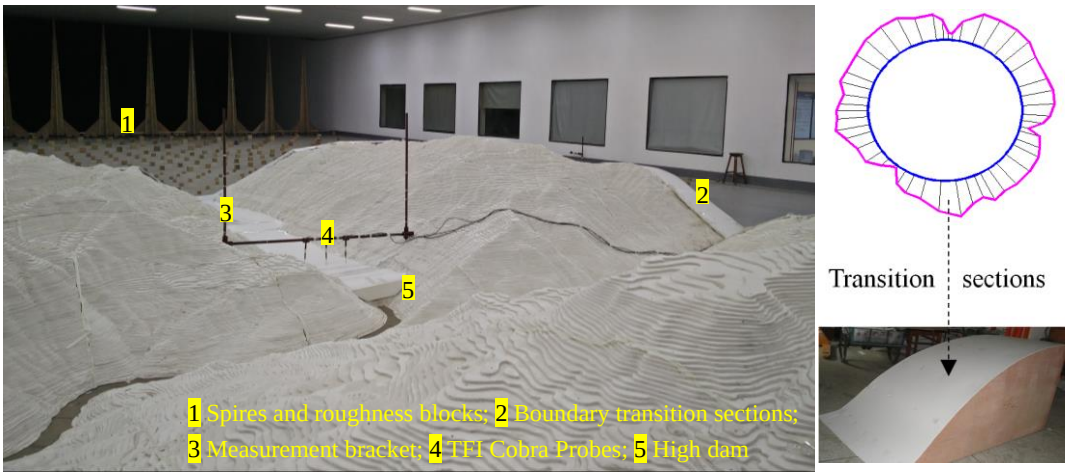

Fig. 3 Terrain model in wind tunnel

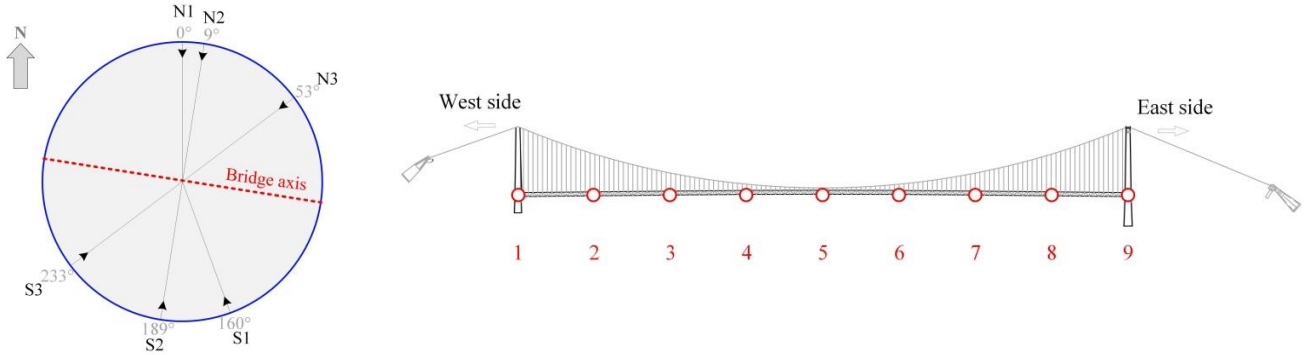

(a) Wind directions set up (b) Layout of measurement points

Fig. 4 Experimental cases

2.3 Effects of the mountains on the wind environment

Fig. 5(a) shows the variations of the angle of attack along the span direction under different wind directions. In general, the absolute value of the angle of attack with south winds is obviously larger than that with north winds. Under north winds, i.e., cases N1, N2, and N3, the variations along the span direction are relatively small and less affected by the wind direction. The probable reason is that the river valley on the upstream side of the bridge is relatively straight. North winds merge into the river and then flow along it, so their non-uniform characteristics are weakened and the absolute values of angle of attack are relatively small. Under south winds, i.e., cases S1, S2, and S3, the angle of attack varies along the span direction significantly and the variation is closely related to the wind direction, which may be caused by the mountain located at the south of the bridge. South winds flow over the mountain and then flow downward to the bridge, making the approaching flow to the bridge show negative angles of attack with larger absolute values.

An anemometer is installed at a distance of 2.73 m from the tunnel ground, corresponding to 6,760 m in the real situation. The measured wind speed is defined as the gradient wind speed U_G, which is little affected by the terrain model. The gradient wind speed ratio is defined as the ratio of the wind speed $U = \sqrt{u^2 + v^2}$ at a certain measurement point to U_G. The variations of the gradient wind speed ratio under different wind directions are shown in Fig. 5(b). It can be observed that the distribution of the gradient wind speed ratio along the span direction is non-uniform. The wind speeds at the two sides of the bridge are lower due to the shelter of the ridges, especially for the west side where the gradient wind speed ratio is lower than 0.4 for all the six cases. The wind speed in the middle part becomes larger, but it is still less than the gradient wind speed. The distribution of the gradient wind speed ratio is affected by the wind direction, and it show more obvious non-uniform characteristics when the wind direction is perpendicular to the bridge axis, i.e., cases S2 and N2. For case S3, the distribution becomes inhomogeneous that the gradient wind speed ratio suddenly decreases at measurement points 3-5, which may be caused by the large-angle bending of the downstream channel of the dam.

Fig. 6 shows the variations of angle of attack and gradient wind speed ratio along the vertical direction. When winds come from the north where the river is relatively straight, the absolute value of the mean angle of attack is small, and increases with the increase in the altitude. When winds come from the south covered by mountains, the incoming flow will cross them and generate a downward subduction trend. Therefore, the absolute values of mean

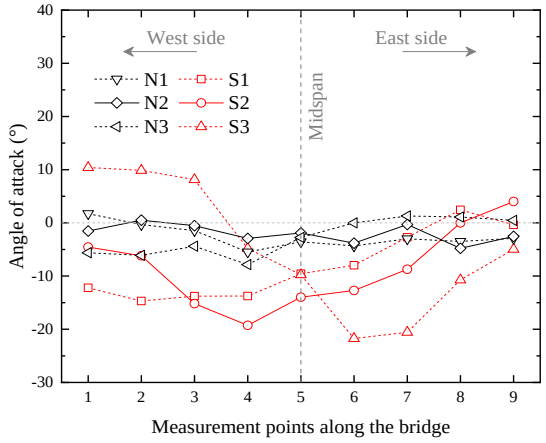

(a) angle of attack

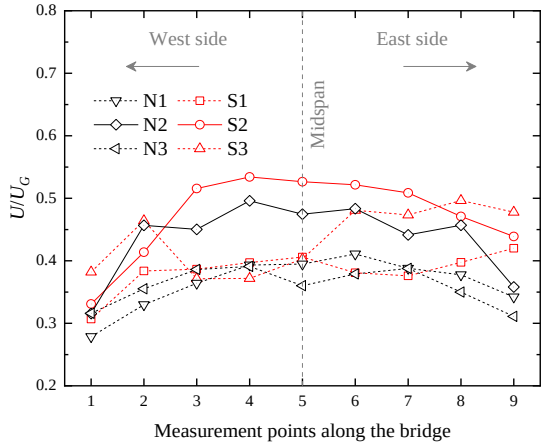

(b) gradient wind speed ratio

Fig. 5 Angles of attack and gradient wind speed ratios along the span direction

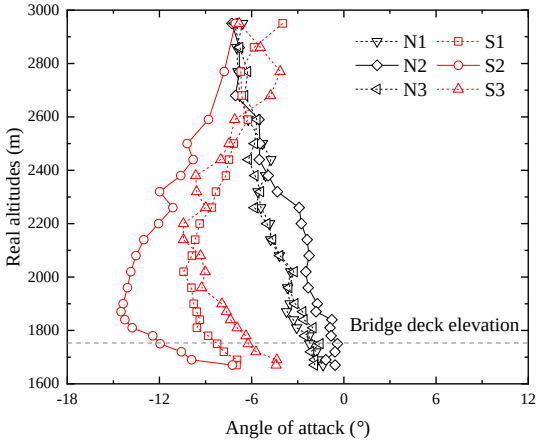

(a) angle of attack

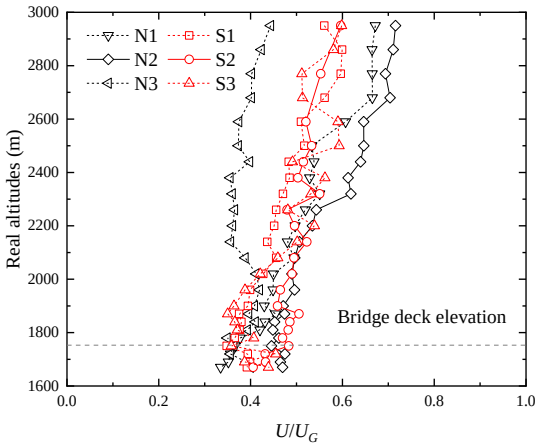

(b) gradient wind speed ratio

Fig. 6 Angles of attack and gradient wind speed ratios along the vertical direction

angle of attack at the bridge deck elevation are larger, and increase first and then decrease with the increase in the altitude (see Fig. 6(a)). Because of the mountain shelter and the frictional action of the slopes surface on both sides of the canyon, the transverse wind speed at the bridge deck elevation is disordered under all wind directions, and the shape of the wind profile at low altitude is not uniform as that at high altitude. When the incoming flow is along the upstream of the river (case N1) or perpendicular to the bridge axis (case N2), the transverse wind speed profile at the bridge site is closer to the traditional exponential law or logarithmic probability profile because the blockage effect for incoming flow of the mountain is relatively small. Under case N3, the increase in transverse wind speed at high altitude is not obvious due to the high mountain shelter in the east and west direction. Under case S2, the transverse wind speed at the bridge deck elevation is the largest. In this situation, the wind profile is inconsistent with the conventional wind profile, showing a S-shape, which is mainly caused by the severe shelter of the southern mountains and the ridges beside the downstream rivers.

2.4 Effects of the dam on the wind environment

In order to understand how the dam affects the wind environment around the bridge site, another two cases were added. The previous case in which the upstream water level behind the dam is 1,420 m was marked by low dam. Increasing the upstream water level, i.e., the height of the dam, to 1,650 m, the case was marked by high dam. Removing the dam, the upstream water level decreased to 1,300 m which is equal to the downstream water level, the case was marked by no dam. Two representative wind directions, i.e. N2 and S2, which are perpendicular to the bridge axis, were taken as the examples.

Fig. 7 shows the effects of the dam height on the angle of attack and the gradient wind speed ratio where the dot lines represent the mean value of the nine measurement points along the span direction. Under the north wind, i.e. N2, the variations of the angle of attack along the span direction are relatively uniform regardless of the dam height. The absolute value of the mean angle of attack increases with the increase in dam height and so does the mean gradient wind speed. Under the south wind, i.e. S2, the non-uniform characteristics of the incoming flow becomes more significant. The angle of attack is greatly affected by the dam height, and the absolute value of mean angle of attack is obviously larger than that with the north wind. Under the high dam, the absolute value of angle of attack is the smallest, probably because the inflow is blocked when

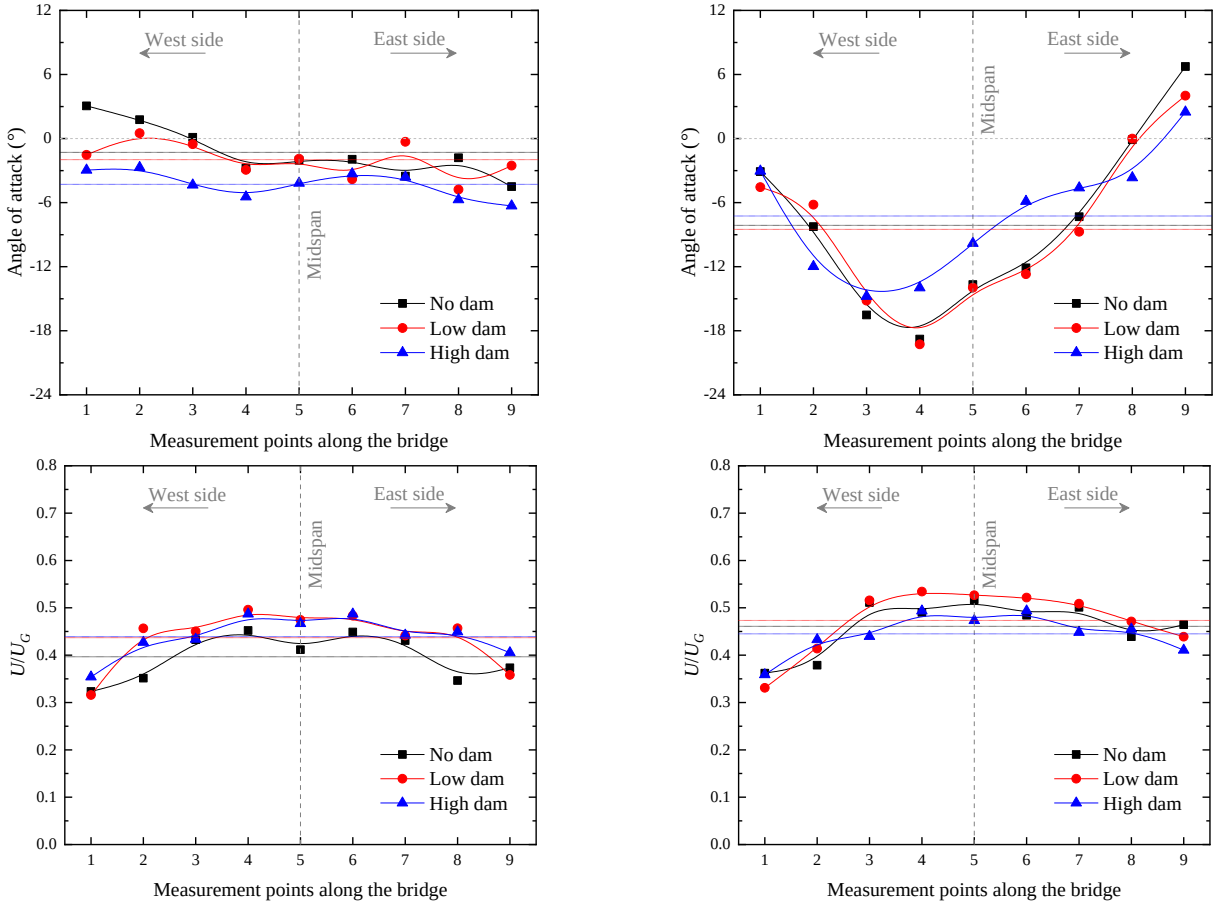

(a) north wind of N2 (b) south wind of S2

Fig. 7 Angles of attack and gradient wind speed ratios along the span direction for different dam heights

passing through the high dam, which climbs upward and weakens the negative angle of attack.

3. Aerostatic stability of the bridge with non-uniform wind environment

3.1 Aerostatic coefficients

The girder is subjected to the drag, the lift, and the pitching moment which are noted by $F_D(\alpha)$, $F_L(\alpha)$, and $F_M(\alpha)$, respectively. The positive directions of the three forces are shown in Fig. 8(a). The aerostatic coefficients in the wind coordinate system are defined as

$$F_D(\alpha) = \frac{1}{2}\rho U^2 C_D(\alpha) HL \tag{1}$$

$$F_L(\alpha) = \frac{1}{2}\rho U^2 C_L(\alpha) BL \tag{2}$$

$$M_T(\alpha) = \frac{1}{2}\rho U^2 C_M(\alpha) B^2 L \tag{3}$$

where ρ is the air density; B and H are the width and the height of the girder, i.e. 27.5 m and 12.2 m, respectively; L is the model length, i.e. 2.095 m; $C_D(\alpha)$, $C_L(\alpha)$ and $C_M(\alpha)$ are the drag, the lift, and the moment coefficients, respectively; U is the wind velocity of the approaching flow. In the following study, the wind velocities are related to the transverse component u only.

The aerostatic coefficients were obtained by sectional model tests in XNJD-1 wind tunnel at Southwest Jiaotong University, and the experimental results are shown in Fig. 8(b).

The tested angle ranged from -12° to 12° with an interval of 1°. The experimental results were fitted by polynomials for the convenience of the interpolation in the following aerostatic analysis. Considering that the target suspension bridge may be attacked by larger angles under south winds, as discussed in section 2.4, the experimental results were extended to a broader range of angles of attack, up to ±18° in magnitude. Fifth-order polynomials were adopted within the range from -12° to 12° to achieve higher fitting precision, while third-order polynomials were adopted for the extrapolated functions to get reasonable trends. The extrapolated functions are used in the parts of sensitivity analysis performed in section 3.3.

3.2 Numerical analysis method

Most of the current methods for calculating aerostatic stability are only applicable to uniform inflow, while the

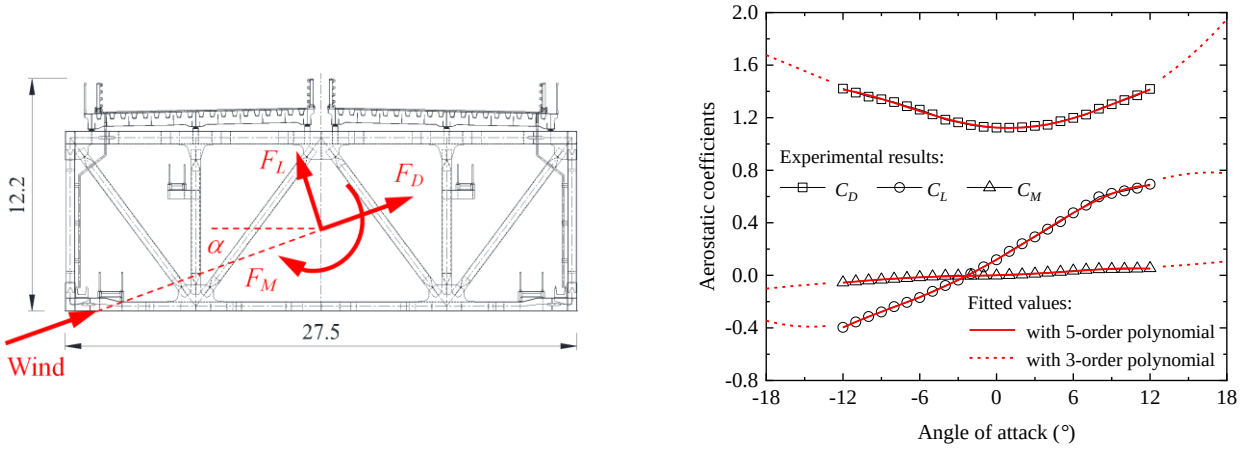

(a) definition of the aerostatic forces (unit: m) (b) aerostatic coefficients

Fig. 8 Mean aerostatic coefficients

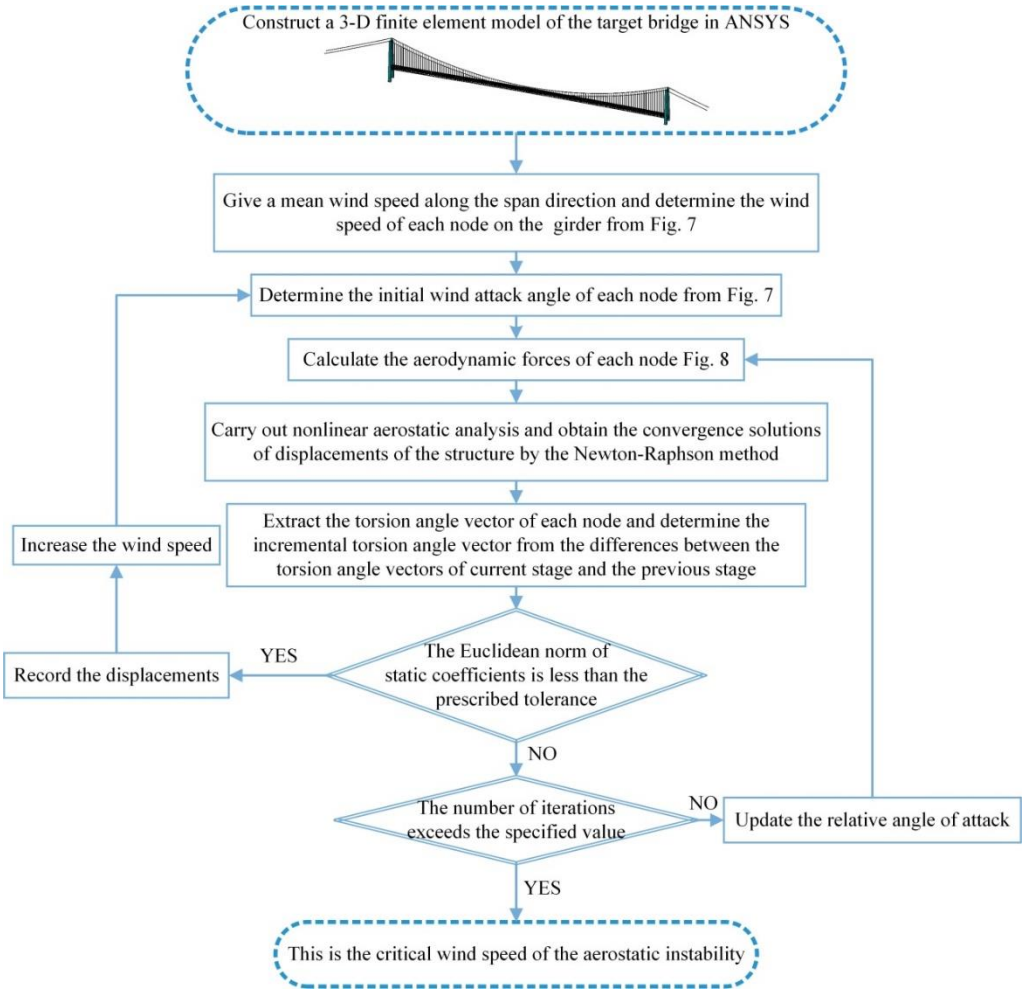

Fig. 9. Nonlinear computational flow chart

method adopted in this paper considers the non-uniform distribution of angle of attack and wind speed along the bridge span direction. At the same time, the non-uniform distribution of wind speed along the vertical direction is also considered. Firstly, the non-uniform distributions of wind speed and angle of attack have been obtained by the terrain model tests. Then, the aerostatic coefficients of the bridge girder have been obtained by the sectional model tests. Considering that the yaw angle has less effect on the critical wind speed of the aerostatic instability of long-span bridges (Zhang et al. 2013a), the variation of the yaw angle is not considered in this paper. It should be noted that the

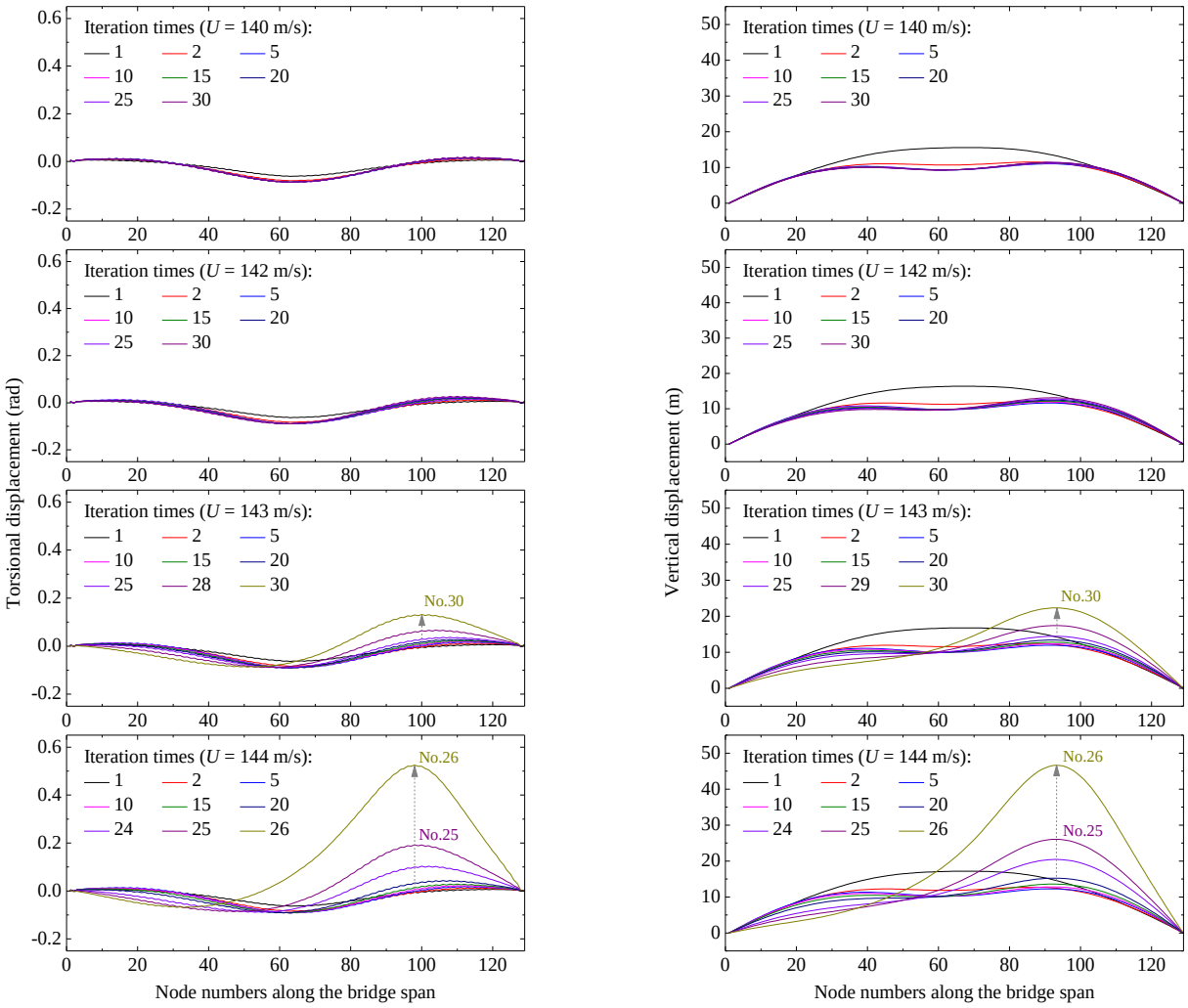

(a) torsional direction (b) vertical direction

Fig. 10 Aerostatic responses of the bridge under uniform incoming flow

wind speed adopted in the calculation is only the resultant wind speed of the transverse component and the vertical component, and its direction is perpendicular to the bridge span. Finally, a cyclic iteration method combining internal and external increments is used to solve the finite element equilibrium equation. Specifically, at a given wind speed, the aerostatic forces applied to the structure are updated by calculating the structural displacement by each iteration, and then the structural displacement is recalculated by the updated aerostatic forces. The convergence of the calculation is judged by the Euclidean norms of the static coefficients under the given wind speed. When the Euclidean norm is small enough, it indicates that the difference of structural displacement calculated by two adjacent iterations is small enough, and the final equilibrium position of the structure has been found. The expression is defined as

$$\left\{\frac{\sum_{i=1}^{N}[C_k(\alpha_i)-C_k(\alpha_{i-1})]^2}{\sum_{i=1}^{N}[C_k(\alpha_{i-1})]^2}\right\} \le \varepsilon_k \tag{4}$$

where N is the total number of nodes that need to apply wind loads, C_k are the static coefficients, ε_k is the allowable tolerance, 10^{-4} is taken in this paper.

The nonlinear calculation program can be realized by APDL technology and the detailed calculation steps are shown in Fig. 9. From the flow chart, it can be found that the initial angle of attack and initial wind speed of each node along the bridge span direction are different, which is different from the traditional aerostatic instability calculation method, and can more truly simulate the wind environment of bridge sites in mountainous terrains.

Taking the uniform inflow with 0° angle of attack as an example, the aerostatic responses of the bridge with different wind speeds are calculated. Similar to the directions of the aerostatic coefficients, the positive displacements in the transverse, the vertical, and the torsional directions are downwind, upward, and nose-up, respectively. During a total of 30 iterations, the variations of the torsional and vertical displacements along the bridge span are shown in Fig. 10. With the iterations, the aerostatic response of the bridge tends to a stable state when the wind speed is lower than 143 m/s. In this situation, the above convergent condition is satisfied, and the aerostatic

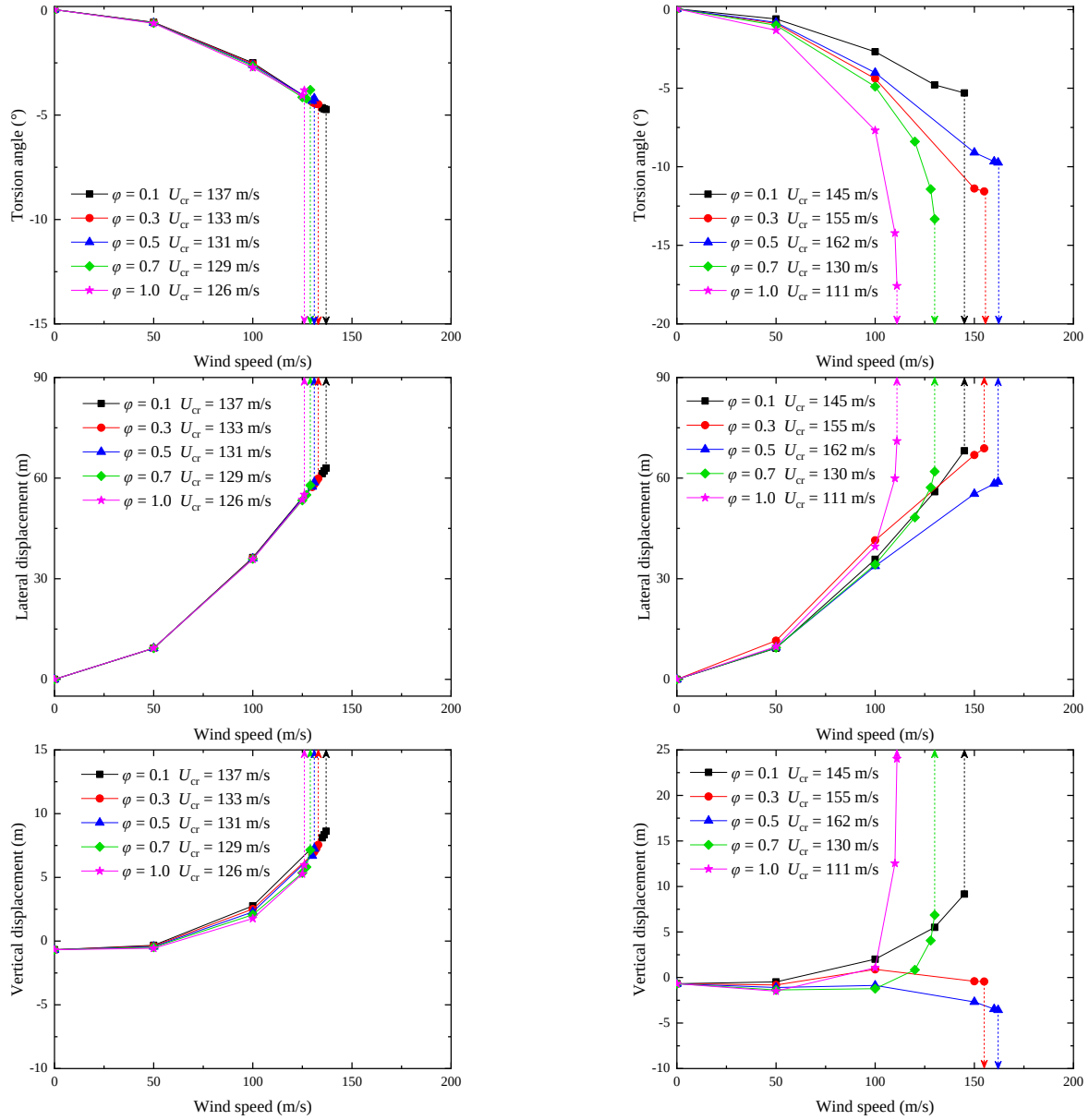

(a) north wind of N2 (b) south wind of S2

Fig. 11 Aerostatic responses at the midspan point under different φ

response of the bridge is stable. When the wind speed is equal to or larger than 143 m/s, however, the aerostatic response of the bridge becomes unstable, for the torsional displacements and the vertical displacements at the east side increase divergently with the iterations. Therefore, the wind speed of 143 m/s is selected as the critical value corresponding to the aerostatic instability of the bridge.

3.3 Effects of non-uniform wind environment on the aerostatic stability

In this section, the aerostatic stability of the suspension bridge with uniform and non-uniform wind environment is studied. Two wind directions, i.e., N2 and S2, are taken into account. The non-uniform wind parameters along the bridge axis refer to the results in Section 2. The computed wind speeds are related to the transverse components. The angles of attack of the incoming flow at some measurement points under the south wind S2 have exceeded the experimental range from -12° to 12°. Moreover, the initial angle caused by the incoming flow will be further increased during the aerostatic analysis. The torsional displacement of the bridge increases with the increase in computed wind speed, leading to larger relative angles between the bridge girder and the incoming flow. In order to avoid using the force coefficients not covered experimentally, the non-uniform angles obtained in Section 2 are systematically multiplied by a reduction factor φ.

Firstly, the sensitivity analysis of non-uniform angles of attack is carried out, and different reduction factors ranging from 0.1 to 1.0 are considered. Here, the wind speed is uniform along the bridge span. When the angle of attack exceeds the experimental range, the extrapolated aerostatic coefficients will be applied. Fig. 11 illustrates the aerostatic

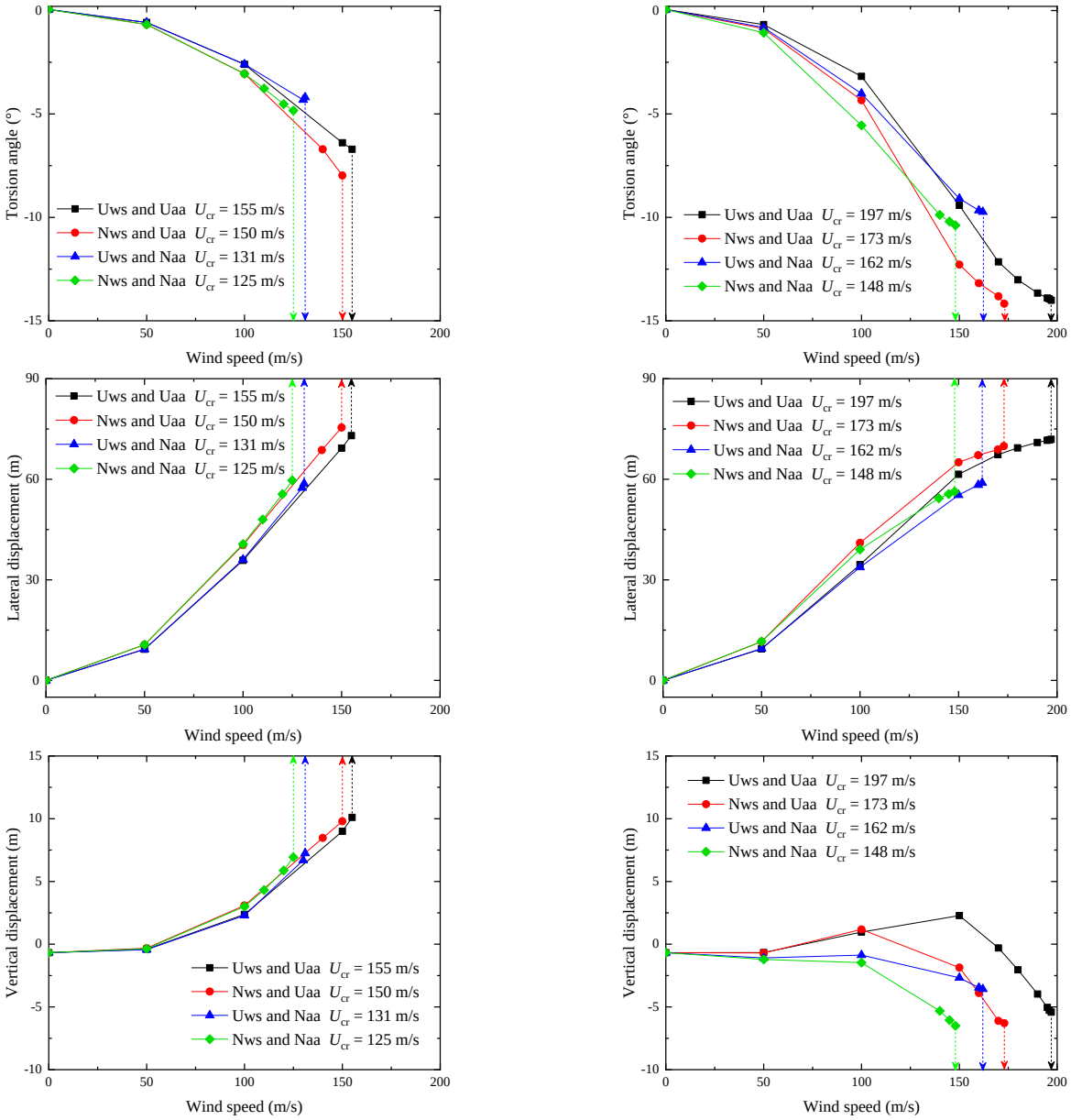

(a) north wind of N2 (b) south wind of S2

Fig. 12 Aerostatic responses at the midspan point under uniform and non-uniform inflow

response of the bridge in the torsional, the lateral, and the vertical directions at the mid-span. The critical wind speed of the aerostatic instability is also given.

Under the north wind of N2, the angle of attack is relatively uniform along the bridge span, and the absolute value is relatively small. The angles of attack of incoming flow around the mid-span are mostly in the range from -3° to 0° where the lift coefficient is positive, while the moment coefficient is negative. As a result, the lift is upward and the moment is counterclockwise, so vertical displacement at the midspan point is positive value, while the torsion angle is negative. With the increase of wind speed, the aerostatic forces increase gradually, leading to the increase of displacement in three directions. With the increase in φ, the critical wind speed of aerostatic instability of the bridge decreases, but the change is limited due to the small absolute value of attack of angle under Case N2. Under the south wind of S2, the effect of the reduction factor on the aerostatic response of the bridge becomes obvious. When φ = 0.1, the angle of attack is small and its distribution is approximately uniform along the bridge span direction. The variations of the torsional, the lateral, and the vertical displacements at the mid-span are similar with the results under Case N2, but the critical wind speed of the bridge increases. When φ increases to 0.3 or 0.5, the non-uniform characteristics of the angle of attack become obvious. It can be seen that the vertical displacement show a different variation versus the computed wind speed. Meanwhile, the critical wind speed of the bridge increases slightly. When φ further increases to 0.7 or 1.0, the rapid change in the displacement makes the aerostatic instability of the bridge occur at lower wind speeds. Although the critical wind

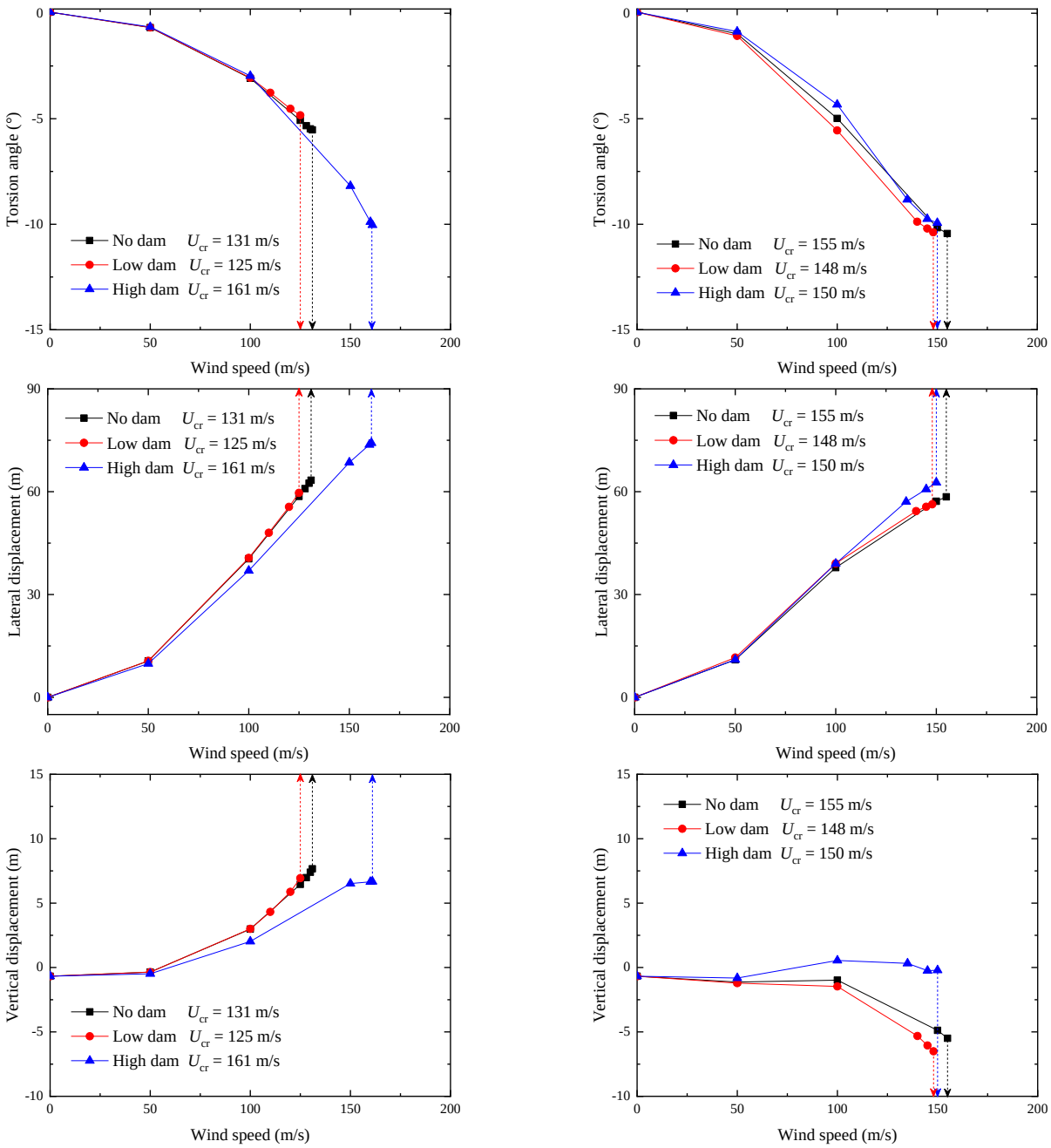

(a) north wind of N2 (b) south wind of S2

Fig. 13 Aerostatic responses at the midspan point for different dam heights

speed of the bridge decreases, the torsional displacement at the mid-span further increases. The superposition of the initial angle of attack caused by the incoming flow and the torsional displacement of the bridge leads to larger relative angles between the bridge girder and the incoming flow. At the aerostatic critical state of the bridge, the relative angles around the mid-span exceed 20° (with φ=0.7) and 30° (with φ=1.0), respectively, at which the flow physics is different than the experimental range, so the reliability of the results decreases.

In general, the effects of φ on the aerostatic response under the south wind is greater than that under the north wind, which may be due to the angle of attack with larger absolute value at the bridge site under the south wind. When φ is taken as 0.5, although there is a deviation from the actual value of critical wind speed, it can reflect the state of aerostatic instability of the bridge under non-uniform incoming flow.

Subsequently, taking low dam as an example, the effects of the non-uniform angle of attack and the non-uniform wind speed on the aerostatic stability of the bridge are studied, where the reduction coefficient is taken as 0.5. For comparison, the aerostatic responses under the four cases, uniform wind speed and uniform angle of attack (Uws and Uaa), non-uniform wind speed and uniform angle of attack (Nws and Uaa), uniform wind speed and non-uniform angle

of attack (Uws and Naa), and non-uniform wind speed and non-uniform angle of attack (Nws and Naa), are illustrated here.

Fig. 12 shows the variations of the torsional, the lateral, and the vertical displacements at the midspan point with the increase in wind speed. Under the uniform incoming flow, the critical wind speed of aerostatic instability under Case N2 and Case S2 is 155 m/s and 197 m/s, respectively, indicating that the critical wind speed is significantly affected by the angle of attack. A single non-uniform factor, angle of attack or wind speed, is unfavorable to the aerostatic stability of the bridge. Compared with the uniform inflow, when the non-uniform wind speed is considered separately, the critical wind speed of Case N2 and Case S2 decreases by 3.2% and 12.2% respectively. The effect of non-uniform wind speed in Case S2 is greater than that in Case N2, which is because the wind speed at the midspan under Case S2 is far higher than the mean wind speed along the bridge span. When the non-uniform angle of attack is considered separately, the critical wind speed of Case N2 and Case S2 decreases by 15.5% and 17.8% respectively. Thus, it can be seen that the effect of non-uniform angle of attack is more significant than that of non-uniform wind speed. Moreover, when the combined action of non-uniform angle of attack and non-uniform wind speed is considered, the critical wind speed of aerostatic instability is further reduced, especially under the south wind of S2. This may be since both the angle of attack and wind speed in the midspan are greater than their mean values under south winds, resulting in a significant increase in the inhomogeneity of wind parameters, which promotes the aerostatic instability.

Finally, the effects of the dam height on the aerostatic stability of the bridge are investigated. Fig. 13 shows the critical wind speed of aerostatic instability and the variation curves of aerostatic responses at midspan point for different dam heights, and the reduction coefficient of angle of attack is still 0.5.

Under the north wind of N2, the paths of aerostatic responses are similar when the dam is not built or the height of the dam is low. With the increase of wind speed, the torsion angle, lateral displacement and vertical displacement increase gradually. Under the case of high dam, however, the critical wind speed of aerostatic instability increases significantly to 161 m/s. At a given wind speed, the absolute values of displacements in all three directions decrease, which may be due to an increase in the absolute value of the mean angle of attack along the span direction. Under the north wind of S2, although the critical wind speed of aerostatic instability varies slightly under different dam heights, the variation of vertical displacement with the wind speed is different. Under the case of high dam, the absolute value of angle of attack at the midspan is obviously smaller than those of the other two cases. As mentioned earlier, the lift coefficient is positive at low wind speed and negative at high wind speed. As a result, the vertical displacement changes from positive to negative with the increase of wind speed. However, when the dam is not built or the height of the dam is low, the absolute value of initial angle of attack is large enough that the vertical displacement is always negative and its absolute value increases with the increase of wind speed.

4. Conclusions

In this paper, the effects of a dam on wind characteristics at a bridge site, and the aerostatic stability of a bridge with non-uniform inflow are investigated. Some conclusions can be made.

- In mountainous areas, the angle of attack and the wind speed show strong non-uniformity along the bridge span direction, and there are obvious differences in different wind direction. For the target bridge, when winds come from the north where the river is relatively straight, the angle of attack is small and its variation along the span direction is relatively limited. With the increase in dam height, the absolute value of the mean angle of attack and the mean gradient wind speed increase. When winds come from the south where the river is winding, the inflow passes through the mountain located at the south of the bridge and then flow downward to the bridge, so the angle of attack varies along the span direction significantly, and the variation is greatly affected by the dam height. The wind speed at the midspan is significantly higher than that at the bridge towers, especially when the direction of inflow is perpendicular to the bridge axis, which is due to the shelter of ridges on both sides.
- A single non-uniform factor, angle of attack or wind speed, is unfavorable to the aerostatic stability of the bridge. Among them, the effect of non-uniform angle of attack is more significant than that of non-uniform wind speed. Moreover, when the combined action of non-uniform angle of attack and non-uniform wind speed is considered, the critical wind speed of aerostatic instability is further reduced, especially under the south wind of S2. This may be since both the angle of attack and wind speed in the midspan are far greater than their mean values under Case N2 when winds are perpendicular to the bridge axis, resulting in a significant increase in the aerostatic forces acting at the midspan of girder, which promotes the aerostatic instability of the bridge.
- When the dam is not built or the height of the dam is low, the aerostatic responses and critical wind speeds of aerostatic instability are similar. Under the case of high dam, however, the critical wind speed of aerostatic instability increases significantly under the north wind of Case N2, and the vertical displacement changes from positive to negative with the increase of wind speed under the south wind of Case S2.
- The paper focuses on the aerostatic performance of the target bridge. It should be noted that the flutter instability of the bridge may occur at lower wind speeds when compared with the aerostatic instability. For long-span bridges in mountainous areas, the effect of non-uniform incoming flow on the flutter performance should be considered. Meanwhile, the effect of aerostatic response should also be considered, because

there is a change in the relative angle between the bridge and the incoming flow.

Acknowledgments

The authors are grateful for the financial supports from the National Natural Science Foundation of China (51708463, 51525804), the Fundamental Research Funds for the Central Universities (2682019CX04).

References

Bilal, M., Birkelund, Y., Homola, M. and Virk, M.S. (2016), "Wind over complex terrain – Microscale modelling with two types of mesoscale winds at Nygårdsfjell", *Renew. Energy*, **99**, 647-653. https://doi.org/10.1016/j.renene.2016.07.042.

Blocken, B., van der Hout, A., Dekker, J. and Weiler, O. (2015), "CFD simulation of wind flow over natural complex terrain: Case study with validation by field measurements for Ria de Ferrol, Galicia, Spain", *J. Wind Eng. Ind. Aerod.*, **147**, 43-57. https://doi.org/10.1016/j.jweia.2015.09.007.

Boonyapinyo V., Lauhatanon Y. and Lukkunaprasit P. (2006), "Nonlinear aerostatic stability analysis of suspension bridges", *Eng. Struct.*, **28**(5), 793-803. https://doi.org/10.1016/j.engstruct.2005.10.008

Cao, S. and Tamura, T. (2006), "Experimental study on roughness effects on turbulent boundary layer flow over a two-dimensional steep hill", *J. Wind Eng. Ind. Aerod.*, **94**(1), 1-19. https://doi.org/10.1016/j.jweia.2005.10.001

Cao, S., Wang, T., Ge, Y. and Tamura, Y. (2012), "Numerical study on turbulent boundary layers over two-dimensional hills - Effects of surface roughness and slope", *J. Wind Eng. Ind. Aerod.*, **104-106**, 342-349. https://doi.org/10.1016/j.jweia.2012.02.022.

Cheng, J., Jiang, J.J., Xiao, R.C. and Xiang, H.F. (2002), "Nonlinear aerostatic stability analysis of Jiang Yin suspension bridge", *Eng. Struct.*, **24**(6), 773-781. https://doi.org/10.1016/S0141-0296(02)00006-8

Cheng, J., Xiao, R.C., Xiang, H.F. and Jiang, J.J. (2003), "NASAB: a finite element software for the nonlinear aerostatic stability analysis of cable-supported bridges", *Adv. Eng. Softw.*, **34**(5), 287-296. https://doi.org/10.1016/S0965-9978(03)00010-3.

Ferreira, A.D., Silva, M.C.G., Viegas, D.X. and Lopes, A.G. (1991), "Wind tunnel simulation of the flow around two-dimensional hills", *J. Wind Eng. Ind. Aerod.*, **38**, 109-122. https://doi.org/10.1016/0167-6105(91)90033-S.

Guignard, F., Lovallo, M., Laib, M., Golay, J., Kanevski, M., Helbig, N. and Telesca, L. (2019), "Investigating the time dynamics of wind speed in complex terrains by using the Fisher–Shannon method", *Physica A*, **523**, 611-621. https://doi.org/10.1016/j.physa.2019.02.048.

Hu, P., Han, Y., Xu, G., Cai, C.S. and Cheng, W. (2019), "Effects of inhomogeneous wind fields on the aerostatic stability of a long-span cable-stayed bridge located in a mountain-gorge terrain", **33**(3), 04020006. *J. Aerospace Eng.*, https://doi.10.1061/(ASCE)AS.1943-5525.0001117.

Hu, P., Li, Y., Huang, G., Kang, R. and Liao, H. (2015), "The appropriate shape of the boundary transition section for a mountain-gorge terrain model in a wind tunnel test", *Wind Struct.*, **20**(1), 15-36. https://doi.org/10.12989/was.2015.20.1.015

Hui, M.C.H., Larsen, A. and Xiang, H.F. (2009), "Wind turbulence characteristics study at the Stonecutters Bridge site: Part I-Mean wind and turbulence intensities", *J. Wind Eng. Ind. Aerod.*, **97**, 22-36. https://doi.org/10.1016/j.jweia.2008.11.002.

Hunt, J.C.R., Leibovich, S. and Richards, K.J. (1988), "Turbulent shear flows over low hills", *Q. J. Roy. Meteor. Soc.*, **114**(484), 1435-1470. https://doi.org/10.1002/qj.49711448405.

Jing, H., Liao, H., Ma, C. and Chen, K. (2019), "Influence of elevated water levels on wind field characteristics at a bridge site", *Adv. Struct. Eng.*, **22**(7), 1783-1795. https://doi.org/10.1177/1369433218825048.

Kim, H.G., Lee, C.M., Lim, H.C. and Kyong, N.H. (1997), "An experimental and numerical study on the flow over two-dimensional hills", *J. Wind Eng. Ind. Aerod.*, **66**(1), 17-33. https://doi.org/10.1016/S0167-6105(97)00007-X.

Li, Y., Hu, P., Xu, X. and Qiu, J. (2017), "Wind characteristics at bridge site in a deep-cutting gorge by wind tunnel test", *J. Wind Eng. Ind. Aerod.*, **160**, 30-46. https://doi.org/10.1016/j.jweia.2016.11.002.

Li, Y., Xu, X., Zhang, M. and Xu, Y. (2017), "Wind tunnel test and numerical simulation of wind characteristics at a bridge site in mountainous terrain", *Adv. Struct. Eng.*, **20**(8), 1223-1231. https://doi.org/10.1177/1369433216673377.

Lystad, T.M., Fenerci, A. and Øiseth, O. (2018), "Evaluation of mast measurements and wind tunnel terrain models to describe spatially variable wind field characteristics for long-span bridge design", *J. Wind Eng. Ind. Aerod.*, **179**, 558-573. https://doi.org/10.1016/j.jweia.2018.06.021.

Mason, P.J. and King, J.C. (1985), "Measurements and predictions of flow and turbulence over an isolated hill of moderate slope", *Q. J. Roy. Meteor. Soc.*, **111**(468), 617-640. https://doi.org/10.1002/qj.49711146818.

Mason, P.J. and Sykes, R.I. (1979), "Flow over an isolated hill of moderate slope", *Q. J. Roy. Meteor. Soc.*, **105**(444), 383-395. https://doi.org/10.1002/qj.49710544405.

Ministry of Transport of the People's Republic of China (2018), "Wind-resistant design specification for highway bridges (JTG/T 3360-01-2018)", Beijing: China Communications Press Co., Ltd. (in Chinese)

Mitsuta, Y., Tsukamoto, O. and Nenoi, M. (1983), "Wind characteristics over complex terrain", *J. Wind Eng. Ind. Aerod.*, **15**(1), 185-196. https://doi.org/10.1016/0167-6105(83)90189-7.

Ren, H., Laima, S., Chen, W.L., Zhang, B., Guo, A. and Li, H. (2018), "Numerical simulation and prediction of spatial wind field under complex terrain", *J. Wind Eng. Ind. Aerod.*, **180**, 49-65. https://doi.org/10.1016/j.jweia.2018.07.012.

Tang, H., Li, Y. and Shum, K.M. (2018), "Flutter performance of long-span suspension bridges under non-uniform inflow", *Adv. Struct. Eng.*, **21**(2), 201-213. https://doi.org/10.1177/1369433217713926.

Wang, Y., Wang, B. and Li, Y. (2017), "Numerical simulation of wind characteristics over bridge site in complicated mountains under the influence of reservoir water storage", *J. Fuzhou University (Natural Science Edition)*, **45**(4), 466-471. (in Chinese). https://doi.org/10.7631/issn.1000-2243.2017.04.0466.

Xiao, R.C. and Cheng, J. (2004), "Advanced aerostatic stability analysis of suspension bridges", *Wind Struct.*, **7**(1), 55-70. https://doi.org/10.12989/was.2004.7.1.055.

Xu, M., Guo, W., Xia, H. and Li, K. (2016), "Nonlinear aerostatic stability analysis of Hutong cable-stayed rail-cum-road bridge", *Wind Struct.*, **23**(6), 485-503. https://doi.org/10.12989/was.2016.23.6.485.

Zhang, W.M., Ge, Y.J. and Levitan, M.L. (2013a), "A method for nonlinear aerostatic stability analysis of long-span suspension bridges under yaw wind", *Wind Struct.*, **17**(5), 553-564. https://doi.org/10.12989/was.2013.17.5.553.

Zhang, W.M., Ge, Y.J. and Levitan, M.L. (2013b), "Nonlinear aerostatic stability analysis of new suspension bridges with multiple main spans", *J Braz. Soc. Mech. Sci. Eng.*, **35**, 143-151. https://doi.org/10.1007/s40430-013-0011-4.

Zhang, X. (2007), "Influence of some factors on the aerodynamic behavior of long-span suspension bridges", *J. Wind Eng. Ind.*

Aerod., **95**, 149-164. https://doi.org/10.1016/j.jweia.2006.08.003.

Zhang, Z.T., Ge, Y.J. and Yang, Y.X. (2013), "Torsional stiffness degradation and aerostatic divergence of suspension bridge decks", *J. Fluid. Struct.*, **40**, 269-283. https://doi.org/10.1016/j.jfluidstructs.2013.05.001.